

# Towards Automated Security Analysis of Smart Contracts based on Execution Property Graph

Kaihua Qin<sup>12\*</sup>, Zhe Ye<sup>23\*</sup>, Zhun Wang<sup>4</sup>, Weilin Li<sup>5</sup>, Liyi Zhou<sup>12</sup>,  
Chao Zhang<sup>4</sup>, Dawn Song<sup>23</sup>, Arthur Gervais<sup>26</sup>

<sup>1</sup>Imperial College London    <sup>2</sup>Berkeley Center for Responsible, Decentralized Intelligence (RDI)

<sup>3</sup>University of California, Berkeley    <sup>4</sup>Tsinghua University

<sup>5</sup>University of Science and Technology of China    <sup>6</sup>University College London

## ABSTRACT

Identifying and mitigating vulnerabilities in smart contracts is crucial, especially considering the rapid growth and increasing complexity of Decentralized Finance (DeFi) platforms. To address the challenges associated with securing these contracts, we introduce a versatile dynamic analysis framework specifically designed for the Ethereum Virtual Machine (EVM). This comprehensive framework focuses on tracking contract executions, capturing valuable runtime information, while introducing and employing the Execution Property Graph (EPG) to propose a unique graph traversal technique that swiftly detects potential smart contract attacks. Our approach showcases its efficacy with rapid average graph traversal time per transaction and high true positive rates. The successful identification of a zero-day vulnerability affecting Uniswap highlights the framework’s potential to effectively uncover smart contract vulnerabilities in complex DeFi systems.

## 1 INTRODUCTION

The rapid expansion and increasing complexity of decentralized finance (DeFi) platforms have amplified the importance of securing smart contracts to mitigate exploits and financial losses. Contemporary approaches for smart contract security audits typically involve the collaboration of automated static analysis tools and manual assessments by security auditors. State-of-the-art static analysis and symbolic execution tools [8, 17–19, 29, 30] have demonstrated efficacy in identifying various security bugs, such as reentrancy, timestamp dependency, and integer overflow/underflow [10]. However, apart from reentrancy, these vulnerabilities do not account for the primary reasons behind most smart contract application exploits [33]. Limitations of these techniques stem from their focus on contract code rather than contract states and their confined scope of analysis, typically restricted to a single contract or DeFi protocol. Additionally, static analysis may have limitations in providing in-depth insights into specific attack vectors. As DeFi systems continue to grow and become more complex, preventing smart contract attacks becomes an increasingly challenging responsibility. Consequently, postmortem analysis has emerged as a vital aspect of smart contract security, aiming to comprehend the attack mechanics and identify vulnerabilities in other contracts or blockchains.

Addressing this challenge necessitates the efficient and in-depth analysis of attack transactions. Traditional platforms such as [etherscan.io](https://etherscan.io) provide only rudimentary information, insufficient for identifying the root cause of an attack. While existing dynamic analysis

solutions demonstrate potential in addressing static analysis limitations, they may focus on specific vulnerabilities only [12, 25] or lack precise data-flow tracking support [7].

The MonoX blockchain project exemplifies this situation. Despite three security audits, the project suffered a successful attack on November 30, 2021. The culprits exploited two vulnerabilities — missing access control validation and opportunity of price manipulation (see Appendix A for a comprehensive case study of the MonoX attack) — which are application-specific and, therefore, unlikely to be identified through static analysis. Additionally, by leveraging a combination of these vulnerabilities, the attackers further complicated detection during manual review processes. Due to the limited extensibility, existing dynamic analysis techniques for smart contracts [12, 25] may not be readily adaptable for analyzing the MonoX attack.

To bridge these gaps, we introduce CLUE, a versatile dynamic analysis framework for smart contracts on the Ethereum Virtual Machine (EVM). CLUE is designed to track smart contract executions and collect valuable runtime information, such as dynamic data, control, and asset flow, providing comprehensive transaction analysis. Leveraging the Execution Property Graph (EPG), a graphic representation of smart contract executions introduced in this work, we propose a graph traversal technique that rapidly extracts potential smart contract attacks from the low-level graphical representation generated by CLUE. Our methodology, centered on the EPG representation, enables concise descriptions and identification of contract vulnerabilities in a more precise and effective manner. The contributions of our work unfold as follows.

- We develop a dynamic smart contract bytecode analysis framework, CLUE, specifically designed for the EVM. Its purpose is to track smart contract executions and gather runtime information such as dynamic data, control, and asset flow. We also introduce the EPG — a comprehensive representation that captures the behavior of smart contract executions.
- Leveraging the EPG, we propose a graph traversal technique that swiftly identifies potential smart contract attacks. This approach extracts semantic information from the low-level graphical representation of an EPG in a transaction under analysis, thereby automating the detection of malicious patterns. The EPG and graph traversal process do not require prior knowledge of the source code, and can seamlessly integrate domain-specific knowledge of analyzed smart contracts to improve vulnerability identification. We implement and assess three graph traversal instances, specifically addressing reentrancy, faulty access control, and price manipulation vulnerabilities. Our evaluation, utilizing

\*Equal contributions.

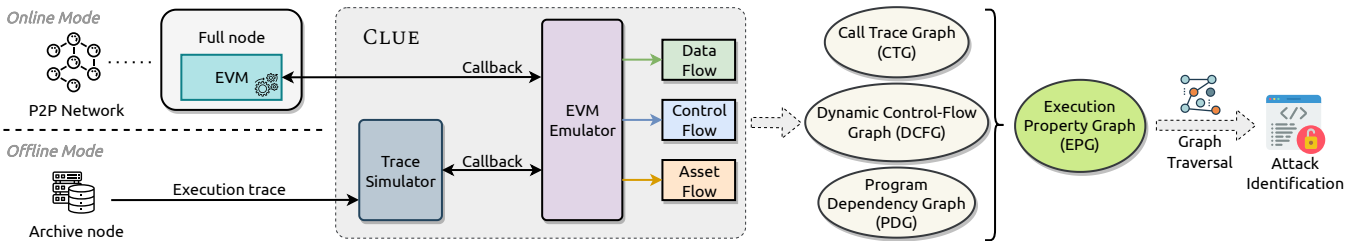


**Figure 1: High-level architecture of CLUE.** CLUE offers support for both online and offline modes. The online mode enables real-time analysis of unconfirmed transactions, while the offline mode facilitates postmortem analysis. Central to CLUE is an EVM emulator, which emulates and tracks the execution of the EVM. CLUE allows extracting the data, control, asset flows from a transaction and further constructing EPG (cf. Section 4) efficiently. Based on the EPG, we devise a graph traversal approach for identifying smart contract attacks automatically (cf. Section 5). We present the implementation details in Appendix B.

a dataset of 63k transactions, demonstrates that the proposed graph traversal takes an average of  $108 \pm 136$ ms per transaction.

- Our framework successfully detected a zero-day vulnerability affecting Uniswap, which we disclosed responsibly. Additionally, CLUE identified 11 reentrancies that had been publicly reported but were not part of our ground truth dataset. Our traversal-based security analysis method achieves high true positive rates of 100%, 75.41%, and 94.44% for reentrancy, faulty access control, and price manipulation, respectively, while maintaining low false positive rates of 0.87%, 5.57%, and 0.52% for these vulnerabilities.

## 2 BACKGROUND

### 2.1 Blockchain and Decentralized Finance

The advent of Bitcoin [20] marked the beginning of a new era of decentralized databases known as blockchains. A blockchain is a peer-to-peer (P2P) distributed database that consists of a series of blocks, each containing a list of transactions. In a blockchain, accounts are represented through unique addresses, and an address can claim ownership of data attributed to it. Every transaction represents a change in the state of the blockchain, such as a transfer of ownership or funds. The blockchain ensures that such ownership transfers are timestamped and agreed upon among the participants. In addition to simple transfers of funds from one address to another, transactions can carry quasi-Turing-complete transition functions, which are realized in the form of so-called smart contracts. Smart contracts in essence are programs running on top of blockchains and allow the implementation of various applications, including financial products, i.e., Decentralized Finance (DeFi). These DeFi applications enable a plethora of use cases, such as financial exchanges [13], lending [22], flash loans [23] and many more.

### 2.2 Ethereum Virtual Machine

Smart contracts are typically executed within a virtual machine (VM) environment. One of the most popular VMs for this purpose is the EVM, which we focus on within this work. EVM supports two types of accounts: (i) the externally owned account (EOA), which is controlled by a cryptographic private key and can be used to initiate transactions, and (ii) the smart contract, which is bound to immutable code and can be invoked by other accounts or contracts.

The code for an EVM contract is usually written in a high-level programming language (e.g., solidity), and then compiled into EVM bytecode. When users want to invoke the execution of a smart contract, they can send a transaction from their EOA to the target contract address, including any necessary parameters or data. An invoked contract can also call other smart contracts within the same transaction, enabling complex interactions between different contracts. EVM utilizes three main components to execute a smart contract: the stack, memory, and storage. The stack and memory are volatile areas, which are reset with each contract invocation, for storing and manipulating data, while the storage is persistent across multiple executions.

While EVM was originally created for the Ethereum blockchain, it has been adopted by a variety of blockchains beyond Ethereum, including BNB Smart Chain and Avalanche. Throughout this work, we focus on the context of Ethereum, but it is worth noting that the contract execution representation EPG and dynamic analysis framework CLUE discussed in this work can also be applied to other EVM-compatible blockchains.

### 2.3 Smart Contract Security

Smart contracts can have bugs and vulnerabilities, just like programs written for traditional systems. Both the academic and the industry communities have therefore adopted tremendous efforts at securing smart contracts. Most of the efforts to date have focused on the smart contract layer, where manual and automated audits aim to identify bugs before a smart contract’s deployment. Despite these efforts, smart contract vulnerabilities have resulted in billions of dollars in losses [33]. As we will explore in this work, detecting and investigating vulnerabilities, forensic in general, is a tedious manual effort that we aim to simplify.

## 3 SMART CONTRACT EXECUTION REPRESENTATIONS

Code representation is a well-studied topic in program analysis literature [3]. Classic code representations, including abstract syntax tree (AST) [1], control-flow graph (CFG) [2], and program dependency graph (PDG) [9], are also applicable to smart contract analysis. Despite their effectiveness in identifying particular contract vulnerabilities [17, 24, 30], these static representations ignore the dynamic

```

1  pragma solidity ^0.8.0;
2  contract Foo {
3      mapping (address => uint) public balances;
4      function withdraw (uint amt) public {
5          uint _balance = balances[msg.sender];
6          if (_balance >= amt) {
7              msg.sender.call{value: amt}("");
8              balances[msg.sender] = _balance - amt;
9          } else {
10             revert("insufficient balance");
11         }
12     }
13 }
14 contract Bar {
15     function callWithdraw(address foo) public {
16         Foo(foo).withdraw(10 ether);
17     }
18     fallback() external payable {
19         if (address(this).balance < 99999 ether) {
20             callWithdraw(msg.sender);
21         }
22     }
23 }

```

**Listing 1: Reentrancy vulnerability example. The contract `Foo` contains a reentrancy vulnerability (line 7 and 8), which an attacker can exploit with the contract `Bar`.**

information exposed in the concrete contract executions, which we aim to capture in this work. Specifically, in the following, we illustrate (cf. Figure 2) how to represent smart contract executions with the (i) call trace graph (CTG), (ii) dynamic control-flow graph (DCFG), and (iii) dynamic dependence graph (DDG).

### 3.1 Running Example

As a running example, we consider a thoroughly studied contract vulnerability, *reentrancy*, which results in the infamous DAO attack [4, 6]. Listing 1 features two contracts, the vulnerable contract `Foo` and the adversarial contract `Bar`. `Foo` allows users to keep a balance of ETH at their address, and also allows withdrawing the deposited ETH. The `withdraw` function, however, performs the withdraw transaction prior to deducting the account balance (line 7 and 8, Listing 1) — and is hence vulnerable to reentrancy. `Bar` exploits the reentrancy through repeated, reentrant calls. An adversary calls the `callWithdraw` function of `Bar` and `Bar` further calls the `withdraw` function of `Foo`. In the `withdraw` function, when `Foo` sends the specified amount of ETH to `Bar` (cf. line 7, Listing 1), the `fallback` function of `Bar` is triggered. This `fallback` function invocation allows repeated ETH withdrawals from `Bar`.

### 3.2 Call Trace Graph

In a transaction, multiple smart contracts can be invoked in a nested and successive manner. We show in our reentrancy example that the contract `Foo` and `Bar` invoke each other repeatedly. Such contract invocations can be structured into a CTG (cf. Figure 2a). Given a transaction, the CTG captures the sequence and hierarchy of contract invocations. Ignoring the detailed executions within a contract, every invocation in a CTG is abstracted into a quintuple: (i) from address — caller; (ii) to address — callee; (iii) invocation opcode — the triggering opcode (cf. Section 4.2.1); (iv) call value — the amount of ETH transferred with the call; (v) call data — call parameters. Call value, the amount of ETH transferred with a contract call,

differentiates the CTG apart from traditional software executions and is key to the specificity of smart contract execution.

Owing to its simplicity, the concept of CTG is extensively employed in contract security analysis, particularly for manual attack postmortem processes. Popular EVM transaction decoders, such as `ethtx.info`, essentially display the CTG of a given transaction to enhance interpretation.

### 3.3 Dynamic Control-Flow Graph

A CFG represents smart contract code as a graph, where each vertex denotes a basic block. A basic block is a piece of contract code that is executed sequentially without a jump. Basic blocks are connected with directed edges, representing code jumps in the control flow.

A CFG is a static representation of contract code, but can also be constructed dynamically while a contract executes, i.e., a so-called DCFG. Figure 2b shows the DCFG of the `Foo` contract (cf. Listing 1) during the reentrancy exploit. Contrary to the CFG, a DCFG focuses on the dynamic execution information, hence ignoring the unvisited basic blocks and jumps. For instance, the code at line 10, Listing 1 is not included in the DCFG (cf. Figure 2b).

### 3.4 Dynamic Dependence Graph

The PDG is another form of code representation outlining the dependency relationship in a program. There are two main types of dependencies, data dependency and control dependency [15]. In this work, for data dependency, we refer to the data flow dependency. An instruction  $X$  has a flow dependency on an instruction  $Y$ , if  $Y$  defines a value used by  $X$ . Note that data flow dependencies are transitive, i.e., if  $Y$  is dependent on  $Z$  and  $X$  is dependent on  $Y$ , then  $X$  is dependent on  $Z$ . We do not consider the other types of data dependencies, such as anti-dependencies [5] and def-order dependencies [14], because they do not apply to contract executions. For control dependency, informally, an instruction  $X$  has a control dependency on a branching instruction  $Y$ , if changing the branch target for  $Y$  may cause  $X$  not to be executed.

Similar to how a DCFG is constructed from concrete executions, a PDG can also be built dynamically, which is referred to as a DDG. We present the DDG of our reentrancy example in Figure 2c, where  $D$  and  $C$  denote data and control dependency, respectively.

### 3.5 Graphs on EVM Bytecode

The graphs in Figure 2 may appear trivial to generate by parsing the transaction execution trace with the smart contract source code. However, EVM only executes bytecode with no knowledge of the high-level code. Furthermore, in practice, a contract is not always open-source. For instance, a reentrancy attacker is unlikely to open-source the exploit contract `Bar`. It is therefore reasonable to build smart contract execution representations based on the bytecode instead of any high-level language.

In this section, we present the reentrancy example (cf. Listing 1 and Figure 2) with solidity to ease understanding. We however clarify that our contract execution representation EPG (cf. Section 4) bases on the EVM bytecode and does not require access to the contract source code. This results in discrepancies between the graphs presented in Figure 2 and the actual graphs. For example,

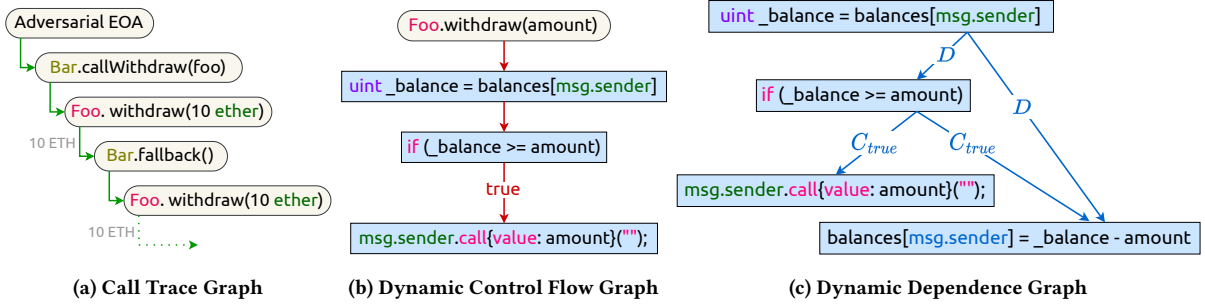


Figure 2: Contract execution representations for the reentrancy example in Listing 1. In Figure 2c,  $C$  and  $D$  indicate control and data dependency respectively.

the nodes in DCFG and DDG should be bytecode basic blocks instead of solidity statements. We defer the details to Section 4.

## 4 EXECUTION PROPERTY GRAPH

In this section, we introduce the EPG as a means to represent and formalize contract executions. The EPG is essentially a property graph that combines the dynamic execution information on the EVM bytecode level, supplied by three basic execution representations, namely CTG, DCFG, and DDG (cf. Section 3). We begin by discussing the fundamentals of property graphs and subsequently formalize the CTG, DCFG, and DDG using property graphs. Lastly, we demonstrate the construction of the EPG by integrating these three basic representations.

### 4.1 Property Graph

A property graph is a multi-relational graph, where vertices and edges are attributed with a set of key-value pairs, known as properties [27]. Contrary to a single-relational graph, where edges are homogeneous in meaning, edges in a property graph are labeled and thus heterogeneous. Properties grant a graph the ability of representing non-graphical data (e.g., different types of relationships between entities in a social network graph). A property graph is formally defined in Definition 4.1.

*Definition 4.1 (Property Graph).* A property graph is defined as  $G = (V, E, \lambda, \mu)$ , where  $V$  is a set of vertices and  $E \subseteq (V \times V)$  is a set of directed edges.  $\lambda : E \rightarrow \Sigma$  is an edge labeling function that labels edges with symbols from the alphabet  $\Sigma$ , while  $\mu : (V \cup E) \times K \rightarrow S$  assigns key-value properties to vertices and edges, where  $K$  is a set of property keys and  $S$  is a set of property values.

In this work,  $K^V$  and  $K^E$  denote the property key sets of vertices and edges respectively, s.t.  $K = K^V \cup K^E$ . We use  $S^k$  to denote the set of property values associated with the property key  $k \in K$ .

### 4.2 Formalizing Basic Representations

We proceed to formalize the three basic execution representations with property graphs.

*4.2.1 Formalizing Call Trace Graph.* A CTG  $G_T = (V_T, E_T, \lambda_T, \mu_T)$  represents the contract invocations within a transaction as discussed in Section 3.2). In a CTG, vertices  $V_T$  correspond to contracts,

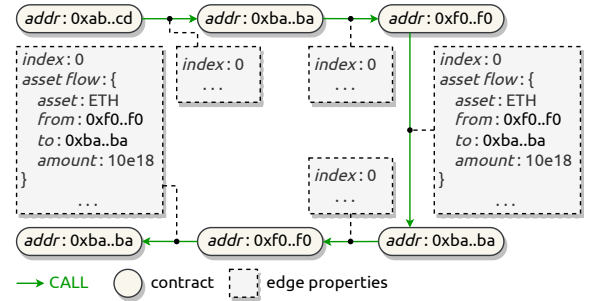


Figure 3: CTG of the reentrancy attack transaction (cf. Section 3.1), where  $0xab..cd$  is the adversarial EOA,  $0xba..ba$  is the adversarial contract `Bar`, and  $0xf0..f0$  is the vulnerable contract `Foo`.

while edges  $E_T$  represent contract invocations from a caller vertex to a callee vertex (cf. Figure 3).

*Vertex.* Every contract vertex  $e_T \in E_T$  is assigned with a property  $addr$  (i.e.,  $K_T^V = \{addr\}$ ) and the associated property value is the contract address.

*Edge.* The labeling function  $\lambda_T$  labels each CTG edge  $e_T \in E_T$  as the opcode triggering this invocation. EVM provides four contract call opcodes and two contract creation opcodes (cf. Equation 1).

$$\Sigma_T = \{\text{CALL}, \text{DELEGATECALL}, \text{CALLCODE}, \text{STATICCALL}, \text{CREATE}, \text{CREATE2}, \text{SELFDESTRUCT}\} \quad (1)$$

Notable, we consider the opcode `SELFDESTRUCT` as a CTG edge. `SELFDESTRUCT` destructs a smart contract and transfers the ETH held by the destructed contract to a specified beneficiary account. The process involves an asset transfer, which we intend to capture in a CTG. A `SELFDESTRUCT` edge starts from the destructed contract vertex and ends in the beneficiary account vertex.

$\mu_T$  assigns five properties (cf. Equation 2) to  $E_T$  as follows.

$$K_T^E = \{index, value, input, output, asset\ flow\} \quad (2)$$

A smart contract can initiate multiple contract calls within a single transaction.  $index$  then indicates the invocation order from a contract vertex.  $value$  is the amount of ETH carried in a contract call.  $input$  and  $output$  are the input parameters and output results

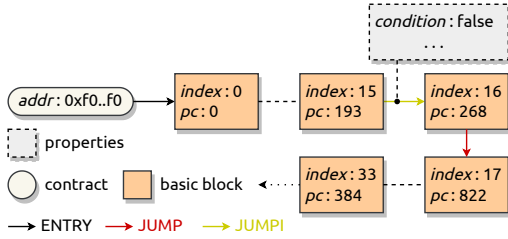


**Figure 4: Partial DCFG of the reentrancy attack transaction (cf. Section 3.1). The JUMPI jump from the basic block at PC 193 to the basic block at PC 268 corresponds to the if conditional statement at line 6, Listing 1.**

of a contract invocation, respectively. *asset flow* specifies the asset transfers following contract calls. There are generally two types of assets in EVM: (i) the native cryptocurrency ETH, and (ii) assets realized by smart contracts (e.g., fungible tokens).  $\mu_T$  hence assigns the *asset flow* property to  $e_T \in E_T$  in the following two scenarios.

- (1)  $e_T$  is associated with a transfer of ETH, i.e.,  $\lambda_T(e_T) \in \{\text{CALL}, \text{CREATE}, \text{CREATE2}, \text{SELFDESTRUCT}\} \wedge \mu_T(e_T, \text{value}) > 0$ .
- (2)  $e_T$  involves transfers of contract-realized assets. The methodology for identifying these transfers is presented in Appendix B.4.

The property value of *asset flow* includes the transferred *asset*, *from*, *to* address, and the transfer *amount*.

**4.2.2 Formalizing Dynamic Control-Flow Graph.** The DCFG aims to capture the control flow within a specific contract execution. When a transaction involves the invocations of multiple contracts (or repeated invocations of a single contract), a DCFG is constructed for each contract execution. It is important to note that, due to the dynamic nature of DCFGs, executing the same contract multiple times may result in different DCFGs. For ease of understanding, the DCFG example in Figure 2b employs solidity statements. However, in EVM bytecode, there is no notion of statements; instead, the control flow of a contract is enabled by jumps between basic blocks of bytecode. Therefore, the DCFG considered in this work consists of basic block vertices, each representing a list of sequentially executed opcodes. To simplify the integration of CTG and DCFG when constructing the EPG (details are outlined in Section 4.3), we design the DCFG to start from a contract vertex, representing the contract under execution (cf. Figure 4).

Formally, a DCFG can be defined as  $G_C = (V_T \cup V_C, E_C, \lambda_C, \mu_C)$ , where  $V_T$  and  $V_C$  represent the contract and basic block vertices respectively. Edges  $E_C$  indicate code jumps between basic blocks.

**Vertex.** Each basic block vertex  $v_C \in V_C$  represents a basic block of EVM bytecode. The property key set for  $V_C$  is  $K_C^E = \{\text{index}, \text{pc}\}$ , where the property  $\text{pc}$  is the entry program counter of the basic block (i.e., the location of the first opcode in the basic block). Because a basic block may be executed multiple times within a single contract execution,  $\text{pc}$  alone is not sufficient to uniquely identify one execution of a basic block. To address this, we introduce the *index* property, an incremental counter that is incremented each time a basic block is visited.

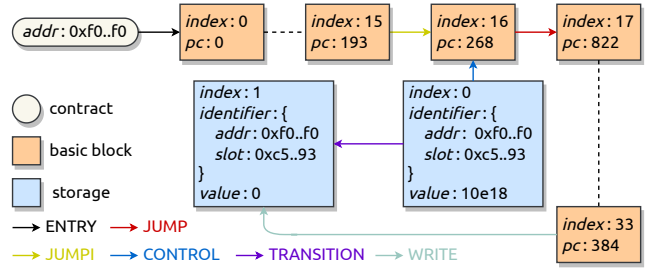


**Figure 5: Partial DDG of the reentrancy attack transaction (cf. Section 3.1). The basic block at PC 384 corresponds to the assignment statement at line 8, Listing 1, where `balances[msg.sender]` is updated.**

**Edge.** An edge  $e_C \in E_C$  in a DCFG represents a code jump between basic blocks. EVM supports two opcodes for code jumps: JUMP (unconditional jump) and JUMPI (conditional jump). A special type of edge, labeled as ENTRY, connects the starting contract vertex  $v_T$  to a basic block vertex  $v_C$  (s.t.,  $\mu_C(v_C, \text{pc}) = 0 \wedge \mu_C(v_C, \text{index}) = 0$ ), indicating the entry of contract execution. In summary, a DCFG can contain three types of edges as outlined in Equation 3.

$$\Sigma_C = \{\text{ENTRY}, \text{JUMP}, \text{JUMPI}\} \quad (3)$$

Every JUMPI edge is assigned with a property *condition* by  $\mu_C$  (i.e.,  $K_C^E = \{\text{condition}\}$ ). The *condition* property indicates the concrete evaluated jump condition value.

**4.2.3 Formalizing Dynamic Dependence Graph.** To capture the dependencies in smart contracts, in the DDG, we consider how various data sources impact contract executions. For example, we intend to capture how the value change of a storage variable impacts a conditional jump (i.e., the JUMPI condition) in the contract execution. There are in general two types of data sources.

**writable data source** The value of a writable data source can change while a contract executes. For example, a storage variable can be written in a contract call. This variable can further impact the subsequent contract executions. Notable, we consider the ETH balance of every account as such a special writable data source, because, similar to a storage variable, the ETH balance of an account can be changed along with contract calls. For these writable data sources, we keep a record of the full change history in the DDG.

**contextual data source** Contextual data sources are read-only, such as call data and block number.

The DDG is built upon the DCFG. Formally, a DDG  $G_D = (V_T \cup V_C \cup V_D, E_D, \lambda_D, \mu_D)$  contains contract vertices  $V_T$ , basic block vertices  $V_C$ , and data source vertices  $V_D$ , while edges  $E_D$  represent the data and control dependencies. Data sources like storage are persistent across contract invocations. Therefore, two DDGs may share the same data source vertices.

**Vertex.** For a writable data source, because we keep a record of its change history, there may exist multiple vertices. A data source vertex has three properties, i.e.,  $K_D^V = \{\text{index}, \text{identifier}, \text{value}\}$ . The *identifier* property uniquely identifies the data source. For example, the contract address and slot hash uniquely identify a storage source. The *index* property serves as history version number, which is

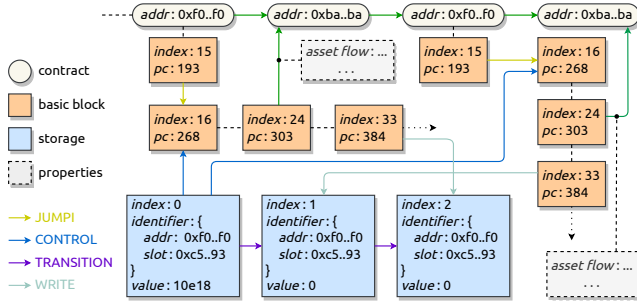


**Figure 6: Partial EPG of the reentrancy attack transaction (cf. Section 3.1).**

incremented every time the data source changes, while the *value* property stores the concrete value of a data source. In the case of a read-only data source, there is only one vertex, and the *index* property is ignored.

*Edge.* There are four types of DDG edges (cf. Equation 4). When a writable data source changes, a new data source vertex  $v_D$  is created. A WRITE edge then connects the basic block vertex  $v_T$ , which contains the opcode performing the data writing operation (e.g., SSTORE), to the newly created vertex  $v_D$ . A control dependency edge, labeled as CONTROL, connects the data source vertex of a JUMPI condition to the target basic block vertex. TRANSITION edges connect the writable data source vertices following an ascending *index* order. If the written content of a data source depends on another data source, they are connected with a DEPENDENCY edge.

$$\Sigma_P = \{\text{WRITE, TRANSITION, CONTROL, DEPENDENCY}\} \quad (4)$$

### 4.3 Constructing the Execution Property Graph

Lastly, the EPG is constructed by merging the three basic property graphs. Because every DCFG originates from a contract vertex and the DDG is built upon the DCFG, the graph merging process is straightforward. The formal definition is provided in Definition 4.2.

*Definition 4.2 (Execution Property Graph).* An EPG  $G = (V, E, \lambda, \mu)$  is constructed by merging CTG, DCFG, and DDG, s.t.,

$$\begin{aligned} V &= V_T \cup V_C \cup V_D \\ E &= E_T \cup E_C \cup E_D \cup T(E_T) \\ \lambda &= \lambda_{T/C/D} \\ \mu &= \mu_{T/C/D} \end{aligned} \quad (5)$$

where  $\lambda_{T/C/D}$  and  $\mu_{T/C/D}$  denote selecting the appropriate labeling and property function accordingly.  $T : V_T \times V_T \rightarrow V_C \times V_T$  is a transformation function, elaborated further in the following.

To incorporate more execution details into the EPG, we apply the transformation function  $T$  to the CTG edges  $E_T$ . For every  $e_T \in E_T$ ,  $T$  generates a new edge  $e'_T$  and inserts into the EPG. The label and properties of  $e'_T$  are inherited from  $e_T$ , while the tail vertex of  $e'_T$  is changed from the caller contract vertex to the basic block vertex initiating the contract invocation. The generated edges enable the EPG to capture contract invocations in a more granular manner.

As an illustration, Figure 6 presents the EPG of the reentrancy attack transaction (cf. Section 3.1), with unnecessary details omitted. From the diagram, it is evident that the balance update (i.e., the storage write) occurs after the ETH transfer, which constitutes the root cause of this reentrancy vulnerability.

## 5 TRAVERSALS BASED SECURITY ANALYSIS

The EPG provides extensive information about the contract executions involved in a transaction. In this section, we explore how graph traversals, a prevalent method for mining information in property graphs, automates the identification of contract attacks. We start with discussing the high-level rationale for security analysis based on EPG traversals. Subsequently, the basics of property graph traversals are outlined. Lastly, we delve into three types of real-world vulnerabilities, reentrancy, faulty access control, and price manipulation.

### 5.1 Rationale

The literature suggests that the primary objective of an individual executing a smart contract attack is typically to obtain financial gain [33]. By exploiting vulnerabilities, an attacker may illicitly acquire financial assets in a way that deviates from the intended design of the compromised contract. As a result, an attack transaction often entails the transfer of assets from the victim to the attacker. To perform a comprehensive security analysis, it is crucial to identify suspicious asset transfers within a transaction. More specifically, a profound understanding of the root cause of a contract attack necessitates an in-depth examination of the underlying mechanisms by which the attacker procures assets from the victim.

For example, in the context of a reentrancy attack (cf. Section 3.1), the attacker can repeatedly invoke a vulnerable contract in a reentrant fashion. To detect such an attack, it is vital to pinpoint the specific asset transfers associated with the reentrant contract calls. Moreover, a reentrancy attack exploits the inconsistent contract state, which is modified subsequent to the malicious asset transfer. The extensive runtime information contained in the EPG enables the detection of suspicious execution patterns, such as reentrant contract invocations and inconsistent contract states. This identification can be achieved by traversing the graph and conducting an appropriate search, as further elaborated in Section 5.3.

We therefore propose a method based on EPG traversals to enable automated transaction security analysis. The goal of traversing the EPG is to infer high-level semantic information from low-level graphic representations and subsequently identify malicious logic patterns. This inference process does not necessitate the knowledge of the application-level logic, rendering the identification methodology more generic and extensible. Nonetheless, for specific vulnerabilities, such as price manipulation, relying solely on graph traversal may result in high false positive rate (FPR) and false negative rate (FNR). To address these vulnerabilities, our methodology also supports integrating corresponding domain knowledge (e.g., estimating price change to detect price manipulation attack) into the traversal process, which can substantially decrease the FPR and FNR. We present the details in Section 6.

## 5.2 Graph Traversal Basics

A traversal refers to the process of visiting vertices of a graph in a specific manner. This process can involve simply visiting every vertex in a predetermined order, or using more sophisticated rules to navigate through the graph. Our formal definition of graph traversal, provided in Definition 5.1, is based on the definition given in [31].

*Definition 5.1 (Traversal).* A traversal of a graph  $G$  is a function  $\mathcal{T} : \mathcal{P}(V) \rightarrow \mathcal{P}(V)$  that maps a set of vertices to another set of vertices, where  $V$  is the vertex set of  $G$  and  $\mathcal{P}(V)$  is power set of  $V$ .

Traversals can be further chained together, denoted by  $\mathcal{T}_1 \circ \mathcal{T}_2$ . We define the elementary traversals as follows.

The filter traversal (cf. Equation 6) returns the nodes in  $X$  that satisfy the predict  $p(v)$ .

$$\text{FILTER}_p(X) = \{v \in X : p(v)\} \quad (6)$$

We also define the following forward and backward traversals. The “out” traversals (cf. Equation 7) return nodes reachable from the set of nodes  $V$  under specific conditions, while the “in” traversals (cf. Equation 8) return nodes that can reach the set of nodes  $V$  under specific conditions.

$$\text{OUT}_I(V) = \bigcup_{v \in V} \{u : (v, u) \in E \wedge \lambda((v, u)) = I\} \quad (7)$$

$$\text{IN}_I(V) = \bigcup_{v \in V} \{u : (u, v) \in E \wedge \lambda((u, v)) = I\} \quad (8)$$

We further define a special traversal  $R_{\mathcal{T}}(V)$  as follows:

$$R_{\mathcal{T}}(V) = \bigcup_{v \in V} \left( \{v\} \cup \left( \bigcup_{v' \in \mathcal{T}(\{v\})} R_{\mathcal{T}}(\{v'\}) \right) \right) \quad (9)$$

$R_{\mathcal{T}}(V)$  recursively applies a traversal  $\mathcal{T}$  on a vertex set  $V$  until the result of traversal  $\mathcal{T}$  returns an empty set.

For example, we can use  $R_{\text{OUT}_T}(V)$  to visit all contract vertices from a contract vertex set  $X$ . When  $V$  is a single vertex set  $v_T$  where  $v_T \in V_T$ ,  $R_{\text{OUT}_T}(V)$  traverses all descendant calls of  $v_T$  in CTG. We let  $\text{TCON}$  be the alias of  $R_{\text{OUT}_T}$  (cf. Equation 10).

$$\text{TCON} = R_{\text{OUT}_T} \quad (10)$$

We define  $R_{\mathcal{T}}^-$ , a useful variant of  $R_{\mathcal{T}}$  which excludes the initial vertex set  $V$ :

$$R_{\mathcal{T}}^-(V) = R_{\mathcal{T}}(V) - V \quad (11)$$

## 5.3 Reentrancy

The concept of reentrancy vulnerability has been well explored in prior research. Specifically, the reentrancy vulnerability is defined by three key characteristics: (i) the presence of reentrant contract calls, (ii) the control of asset transfers relying on outdated storage values, and (iii) storage updates subsequent to asset transfers [25]. In the following, we introduce a method for identifying reentrancy vulnerabilities with EPG traversals.

We provide an overview of the traversals depicted in Figure 7. The traversals initially identify the occurrence of a reentrant invocation, subsequently collect all basic blocks that write to the

control data source of the child invocation, and ultimately ascertain whether these basic blocks are executed following the child invocation.

To identify reentrant contract invocations, we define the traversal  $\text{REENTRANT}$

$$\text{REENTRANT}(\{v_T\}) = \text{FILTER}_p \circ \text{TCON}(\{v_T\}) \quad (12)$$

where  $p$  is a predicate returning true if  $\mu(v, \text{addr}) = \mu(v_T, \text{addr})$ .

Given a specific reentrant pair  $(v_0, v)$  where  $v \in \text{REENTRANT}(\{v_0\})$ , we can determine if it is a reentrancy attack by examining all storage control in  $v$ . Given a specific storage control in  $v$ , we need to find the set of basic blocks  $V_{\text{control}}$  that write to the same storage slot. If there exists a basic block  $b \in V_{\text{control}}$  which (i) belongs to a descendant call of  $v_0$  or  $v_0$  itself; (ii) does not belong to a descendant call of  $v$  or  $v$  itself; (iii) is executed after  $v$ , then we can know that a reentrancy attack happens.

Let  $CT$  be the label of edges transformed by  $T$  (cf. Equation 5). We define a traversal  $\text{CONTROLBLOCK}$  (cf. Equation 13) which find  $V_{\text{control}}$ , i.e.  $V_{\text{control}} = \text{CONTROLBLOCK}(\{v\})$ .

$$\begin{aligned} \text{CONTROLBLOCK} = & \text{IN}_{\text{WRITE}} \circ \text{OUT}_{\text{TRANSITION}} \\ & \circ \text{IN}_{\text{CONTROL}} \circ \text{R}_{\text{OUT}_{CT,CT}} \end{aligned} \quad (13)$$

The  $\text{CONTROLBLOCK}$  traversal first starts with  $\text{R}_{\text{OUT}_{CT,CT}}$ , which finds all descendant calls of  $v$  along with their basic blocks in DCFG. Then,  $\text{IN}_{\text{CONTROL}}$  gives all the data sources that can control these basic blocks and  $\text{IN}_{\text{WRITE}} \circ \text{OUT}_{\text{TRANSITION}}$  finds all basic blocks that write to these data sources.

Given a call  $v' \in \text{OUT}_T(\{v\})$ , i.e. a direct child call of  $v_0$ , we define a traversal  $\text{SUCCBLOCK}_1(\{v'\})$  that finds all basic blocks of descendant calls of  $v_0$  which are executed after  $v'$ 's completion:

$$\text{SUCCBLOCK}_1 = \text{FILTER}_{p_C} \circ \text{R}_{\text{OUT}_{CT,CT}}^- \circ \text{IN}_{CT} \quad (14)$$

First,  $\text{IN}_{CT}$  finds the basic block in  $v_0$  where  $v'$  is called, then  $\text{FILTER}_{p_C} \circ \text{R}_{\text{OUT}_{CT,CT}}^-$  outputs all descendant calls after that basic block, where predicate  $p_C$  holds iff  $\lambda(v) \in \lambda_C$ . Notice we use  $\text{R}_{\text{OUT}_{CT,CT}}^-$  to exclude the basic block where  $v'$  is called.

However, if  $v'$  is not a direct child call of  $v_0$ ,  $\text{SUCCBLOCK}_1$  cannot find basic blocks in  $v_0$  after  $v'$ 's completion. We relax this constraint in  $\text{SUCCBLOCK}_{\rightarrow v_0}(\{v'\})$ :

$$\text{SUCCBLOCK}_{\rightarrow v_0}(\{v'\}) = \text{SUCCBLOCK}_1(\text{R}_{\text{IN}_T}(\{v'\}) - \text{R}_{\text{IN}_T}(\{v_0\})) \quad (15)$$

Here  $\text{R}_{\text{IN}_T}(\{v'\}) - \text{R}_{\text{IN}_T}(\{v_0\})$  outputs all the calls between  $v'$  and  $v_0$ , including  $v'$  but excluding  $v_0$ . Note that if  $b$  is belongs to  $\text{SUCCBLOCK}_{\rightarrow v_0}(\{v'\})$ , it must also be the basic block inside call  $v_0$  or its descendant, i.e.:

$$b \in \text{SUCCBLOCK}_{\rightarrow v_0}(\{v'\}) \implies b \in \text{R}_{\text{OUT}_C}^- \circ \text{TCON}(\{v_0\})$$

Given these traversals, we can formally define the condition of reentrancy attacks:

$$\begin{aligned} \exists v_0, v \in V_T, b \in V_C : & v \in \text{REENTRANT}(\{v_0\}) \\ & \wedge b \in \text{CONTROLBLOCK}(\{v\}) \\ & \wedge b \in \text{SUCCBLOCK}_{\rightarrow v_0}(\{v\}) \end{aligned} \quad (16)$$

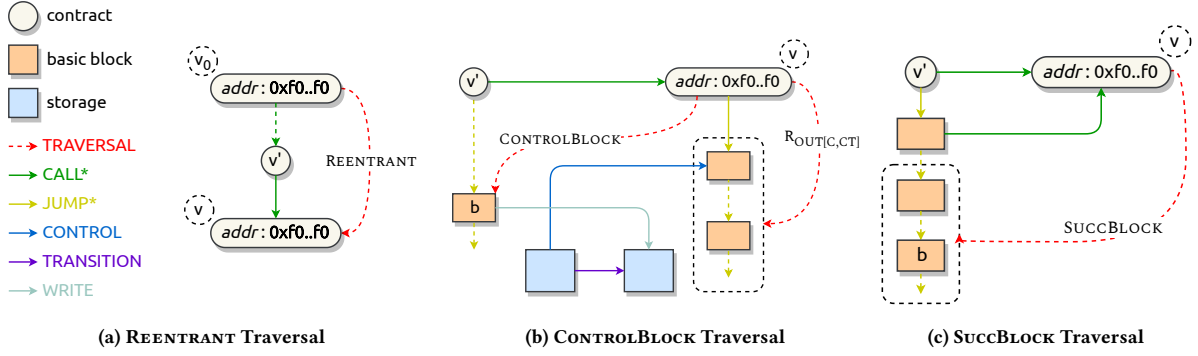


**Figure 7: Three traversal components of the reentrancy attack detection.** CALL\* represents all edge labels of  $E_T$  and  $E_{CT}$ , JUMP\* represents all edges of  $E_C$ . Except TRAVERSAL, dotted edges represent one or more edges with internal vertices omitted. TRAVERSAL edges represent the result of traversal execution.

It is important to note that our traversal approach covers all three types of reentrancy vulnerabilities (i.e., cross-contract, delegated, create-based reentrancy) discussed in [25], as EPG uses a unified model to capture all types of contract calling.

#### 5.4 Faulty Access Control

Access control in smart contracts often involves the verification of the contract caller. As a result, it is feasible to identify the absence of access control by examining the presence of control flow involving the caller. With the CONTROL edges in the EPG, checking the control data sources allows inspecting whether a control flow includes the caller verification. Note that we exclude the control flows unrelated to asset transfers.

We define CONTROLSOURCE (cf. Equation 17) which returns all the relevant control data sources of a specific basic block.

$$\text{CONTROLSOURCE} = R_{\text{INDEPENDENCY}} \circ \text{IN}_{\text{CONTROL}} \circ R_{\text{IN}_{\text{C,CT}}} \quad (17)$$

Given a basic block,  $R_{\text{IN}_{\text{C,CT}}}$  finds all basic block executed before it, and  $R_{\text{INDEPENDENCY}} \circ \text{IN}_{\text{CONTROL}}$  outputs all relevant control data sources of these blocks.

Let  $V_{\text{transfer}}$  be the set of basic blocks that have asset transfers. We can obtain  $V_{\text{transfer}}$  by the following traversal:

$$V_{\text{transfer}} = \text{FILTER}_{\text{HasTransfer}} \circ \text{IN}_{\text{CT}}(V_T) \quad (18)$$

where the predicate *HasTransfer* is defined as follows:

$$\text{HasTransfer}(b) = b \in V_C \wedge \bigcup_{v_T \in \text{OUT}_{\text{CT}}(\{b\})} \mu((b, v_T), \text{asset flow}) \neq \emptyset \quad (19)$$

Given  $V_{\text{transfer}}$  and CONTROLSOURCE, we can formally define the condition of faulty access control:

$$\exists b \in V_{\text{transfer}} : v_{\text{ORIGIN}} \notin \text{CONTROLSOURCE}(\{b\}) \quad (20)$$

#### 5.5 Price Manipulation

A price manipulation attack refers to the malicious exploitation of vulnerabilities in smart contracts for the purpose of manipulating asset prices, generally achieved by tampering with price oracles. In cases where a price manipulation attack occurs within a single transaction, the attacker can alter the price, typically stored in the contract storage, and subsequently profit by, for instance, exchanging assets at the manipulated price. This type of attack transaction entails an asset transfer, the amount of which relies on the manipulated storage.

Our price manipulation traversal then attempts to search such asset transfers that are “influenced” by previous storage changes. It first identifies all possible control data sources of asset flows using CONTROLSOURCE, and then finds all basic blocks that write to the aforementioned data sources (INWRITE) and their related control data sources. The traversal is defined in Equation 21.

$$\text{WRITECONTROL} = \text{CONTROLSOURCE} \circ \text{IN}_{\text{WRITE}} \circ \text{CONTROLSOURCE} \quad (21)$$

The price manipulation attack condition is shown in Equation 22.

$$\exists b \in V_{\text{transfer}} : v_{\text{ORIGIN}} \notin \text{WRITECONTROL}(\{b\}) \quad (22)$$

## 6 EXPERIMENTAL EVALUATION

In this section, we evaluate the performance of EPG traversals in identifying smart contract attacks.

### 6.1 Evaluation Design

**6.1.1 Implementation.** We implement a prototype of the CLUE framework (cf. Figure 1), including the transaction trace simulator, EPG construction, and graph traversal, totaling 6,077 lines of code (LoC) in Golang. Specifically, the transaction trace simulator is implemented using 661 (11.7%) LoC. The three flow tracking modules of CLUE are implemented with 3,019 (53.3%) LoC, while the graph construction module is implemented with 1,984 (35.0%) LoC. We utilize Apache TinkerGraph as our graph backend, which is connected to CLUE through the WebSocket protocol within a

local network. The graph traversal employs the Golang binding of the Gremlin [26] language with a total of 413 LoC.

**6.1.2 Setup.** The evaluation is conducted on an Ubuntu v22.04 machine, equipped with 24 CPU cores and 128 GB of RAM.

**6.1.3 Augmented Dataset.** For the evaluation, we construct three separate datasets: (i) an attack, (ii) a high-gas and (iii) a regular transaction dataset. The datasets are based on an augmented reference dataset, which originates from the work of Zhou *et al.* [33], containing 2,452 DeFi attack transactions on Ethereum. We focus on the three most common types of smart contract attacks: (i) reentrancy, (ii) faulty access control, and (iii) price manipulation, with 87, 61, and 54 attack transactions, respectively.

To enhance the dataset, we collect all transactions that have interacted with the related victim contracts between block 9193268 (1st of January, 2020) and 14688629 (30th of April, 2022), resulting in 4,786,542 transactions that are not classified as attacks for comparative analysis. For each vulnerability type, we create the following three subsets of transactions:

**Attack dataset** The *Attack* dataset comprises all attack transactions that were reported in [33] and correspond to the evaluated vulnerability type. Its main objective is to assess the true positive rate and FNR, as well as to gain an understanding of the reasons behind misclassification.

**Non-attack datasets** The non-attack datasets aim to evaluate CLUE’s performance on benign transactions. To this end, all attack transactions are manually removed from the following two datasets when sampling transactions. The primary objective is to assess the true negative rate and FPR.

- *High-Gas*: As attack transactions often consume more gas due to complex actions, the *High-Gas* dataset initially comprises the top 1,100 transactions with the highest gas consumption. After removing the attacks, this dataset represents complex execution logic, evaluating performance on benign transactions that could be misclassified as attacks.
- *Regular*: The *Regular* dataset initially contains 20,000 randomly selected transactions. After removing true positives, it reflects typical non-attack transactions.

**6.1.4 Limitations.** The evaluation design presents certain limitations regarding the scope of vulnerabilities, dataset dependency, and time performance estimation. First, our evaluation focus on the three most common vulnerability types. We, however, remark that the CLUE framework remains generic. Second, the dependency on Zhou *et al.*’s dataset [33] as ground truth could introduce biases, as it may contain errors and cannot capture all real-world attack scenarios. To mitigate these biases, we employ manual inspections in our evaluation.

## 6.2 Reentrancy

Table 1 presents the evaluation results of the reentrancy attack identification using the *Attack*, *High-Gas*, and *Regular* datasets. CLUE effectively detects reentrancy attacks with a low FNR of 8.05% in the *Attack* dataset and a low false-positive rate of 0.19% and 0.005% in the *High-Gas* and *Regular* datasets, respectively.

**Table 1: Reentrancy evaluation. The *Attack* dataset shows a high true positive rate (91.95%) and a relatively low false negative rate (8.05%) with all false negatives resulting from "No Asset Flow" cases. In non-attack datasets, the true negative rates are remarkably high (99.81%) for *High-Gas* and (99.99%) for *Regular*. The few false positives are caused by Flash Loan and Rebase Token cases.**

Dataset	<i>Attack</i>	Non-attack	
		<i>High-Gas</i>	<i>Regular</i>
Size	87	1,077	19,985
Gas Cost	3.33 ± 3.41M	2.13 ± 1.38M	0.24 ± 0.29M
Generic Rule (cf. Section 5.3)			
Traversal Time	108 ± 136ms	20 ± 21ms	7 ± 3ms
TP (%)	80 (91.95%)	-	-
FN (%)	7 (8.05%)	-	-
No Asset Flow	7 / 7	-	-
TN (%)	-	1,075 (99.81%)	19,984 (99.99%)
FP (%)	-	2 (0.19%)	1 (0.01%)
Flash Loan	-	2 / 2	0 / 1
Rebase Token	-	0 / 2	1 / 1
Refined Rule (Generic Rule + Refinement R1)			
Traversal Time	0.32 ± 0.93s	52 ± 109ms	16 ± 347ms
TP (%)	87 (100%)	-	-
FN (%)	0 (0%)	-	-
TN (%)	-	1,069 (99.26%)	19,812 (99.13%)
FP (%)	-	8 (0.74%)	173 (0.87%)

Notably, CLUE successfully discovers 11 *new* reentrancy transactions within the *Regular* dataset. These transactions are confirmed as true positives that had been missed in the *Attack* dataset from [33]. We have reported these missed true positives to the authors, who have acknowledged the findings and confirmed their intent to address them in the next revision of their work.

**6.2.1 Zero-day Vulnerability Discovery - imBTC Reentrancy.** After further investigation of these 11 newly discovered reentrancy transactions, we discover a potential vulnerability in token *imBTC*.<sup>1</sup> The attacks under investigation commence with the utilization of *imBTC* to exchange for ETH within the Uniswap V1 pool. Subsequently, the attacker exploits the callback function during the transfer of *imBTC* as an ERC777 token, initiating a reentrancy attack. This enables the attacker to execute another exchange with inaccurate pricing prior to the liquidity pool update, ultimately yielding a profit. The fundamental cause of these attacks can be ascribed to the discrepancy between the Uniswap V1 standard and the ERC777 standard. Through further analysis of *imBTC*, our research uncovers potential attack vectors within Uniswap V2 as well. In accordance with responsible disclosure practices, we have reported these findings to the developers and have received prompt and constructive responses.<sup>2</sup>

<sup>1</sup>*imBTC* token address: 0x3212b29E33587A00FB1C83346F5dBFA69A458923

<sup>2</sup>As the vulnerability has not yet been addressed, we are unable to provide further details in this submission.

**6.2.2 False Negative Analysis for Attack Dataset.** In assessing the *Attack* dataset, the false negatives can be attributed to the FeiProtocol incident. Upon manual examination, all false negative instances can be classified as a single type – *no asset flow reentrancy*, which is an atypical reentrancy pattern and hence beyond the scope of the traversal rule outlined in Section 5.3. We further extend the CLUE framework below by adding refinement rules to address this issue.

**6.2.3 Refinement R1 - Status Change based Reentrancy Detection.** The traversal rule defined in Section 5.3 fails to identify this attack due to the lack of asset flow in the reentrant call. To better capture such attacks, we propose a new refinement rule for reentrancy attack detection. The new refinement R1 takes into account the unexpected status changes in a reentrant call, expanding the detection capabilities of the original traversal rule. While R1 successfully identifies all the transactions in the *Attack* dataset, it introduces a significant time overhead, which is about 2.9× on average compared to the time required by the original rule.

**6.2.4 False Positive Analysis for Non-Attack Dataset.** In analyzing the *High Gas* and *Regular* datasets, CLUE identifies 2 out of 1,077 and 1 out of 19,985 benign transactions as reentrancy attacks, respectively (i.e., false positives). Consequently, the FPR amounts to 0.19% and 0.01% in the *High-Gas* and *Regular* datasets, respectively. Both false-positive cases from the *High-Gas* dataset are associated with the flash loan process in Euler Finance. The callback function tied to the flash loan creates a reentrant call pattern. Furthermore, there are some special variables related to the state of borrowing and repayment. They are changed both when borrowing and repayment, and affect the control flow and the asset flow. This issue can be resolved by verifying the from and to addresses of the suspicious asset flow. The single false-positive case from the *Regular* dataset also interacts with another rebase token similar to imBTC as we described in section 6.2.1. It triggered a reentrant call from Uniswap V2 router when performing a transfer to swap and add liquidity. However, there is no potential vulnerability in this situation as the caller is limited to Uniswap V2 router.

**6.2.5 Summary.** CLUE demonstrates a high level of effectiveness in detecting reentrancy attacks, including previously undiscovered attack instances. As for false negatives, the extensibility of EPG facilitates the development of new rules to accurately recognize emerging attack patterns. In the case of false positives, they can either be rapidly filtered out or utilized as indicators of potentially risky behavior that merits further scrutiny.

### 6.3 Faulty Access Control

Table 2 presents the evaluation results of faulty access control attack identification using the *Attack*, *High-Gas*, and *Regular* datasets. In summary, CLUE identifies 46 out of 61 transactions as faulty access control attacks in the *Attack* dataset, resulting in a FNR of 24.59%.

**6.3.1 False Negative Analysis for Attack Dataset.** Our experiment yields 23 FNs for faulty access control attack detection. Upon further inspection, we categorize the FNs into two types:

**6.3.2 Refinement A1 - FN Caused by Access Control within the Attack Contract.** 8 of the false negatives result from the attacker’s access control within the attack contract, which seemingly covers

**Table 2: Faulty access control evaluation. The *Attack* dataset demonstrates a high true positive rate (75.41%) and a low false negative rate (24.59%), with all false negatives being multi-transaction cases. In non-attack datasets, the true negative rates are remarkably high (98.44%) for *High-Gas* and (94.43%) for *Regular*. The few false positives stem from complex DeFi transactions and insufficient authorization checks.**

Dataset	Attack	Non-attack	
		High-Gas	Regular
Size	61	1,091	19,992
Gas	0.22 ± 0.65M	2.21 ± 1.53M	0.24 ± 0.28M
Generic Rule (cf. Section 5.4)			
Traversal Time	9 ± 18ms	0.7 ± 8.6s	13 ± 244ms
TP (%)	38 (62.30%)	-	-
FN (%)	23 (37.70%)	-	-
Multi-tx	15/23	-	-
Attacker contract	8/23	-	-
TN (%)	-	942 (86.34%)	14,850 (74.28%)
FP (%)	-	149 (13.66%)	5,142 (25.72%)
Refined Rule (Generic Rule + Refinement A1, A2, A3)			
Traversal Time	48 ± 121ms	8 ± 47s	0.08 ± 3.07s
TP (%)	46 (75.41%)	-	-
FN (%)	15 (24.59%)	-	-
Multi-tx	15/15	-	-
TN (%)	-	1,074 (98.44%)	18,879 (94.43%)
FP (%)	-	17 (1.56%)	1,113 (5.57%)

the asset flow in the victim contract, leading to false negatives. This is because the attacker’s access control in the outer layer of the attack contract implies that only the attacker can execute the attack, making it appear as if the victim contract’s asset flow is protected by access control as well. To address this issue, we introduce refinement A1, which refines our traversal rule based on this observation and successfully eliminates these 8 false negatives. In refinement A1, we explicitly exclude control data sources inside attacker contracts.

**6.3.3 FN Caused by Multi-Transaction Attacks.** The remaining 15 false negatives are associated with the DaoMaker attack[28], in which the attacker executes the attack across multiple transactions. As a concrete example, in the first transaction, the attacker gains control of the contract through a function with faulty access control, and in the second transaction, transfers all the contract’s assets. We contend that this type of attack is beyond the scope of CLUE, as CLUE is currently designed for single transaction analysis.

**6.3.4 False Positive Analysis for Non-Attack Dataset.** In the *High-Gas* and *Regular* datasets, false positives are primarily attributed to the complex and diverse access control mechanisms employed in DeFi applications. The initial experiment yields a false positive rate (FPR) exceeding 25%. To mitigate the FPR, we introduce two targeted refinements. The combination of these two refinements allows us to reduce the false positive rate to approximately 5%. While we believe that additional refinements could further decrease the FPR, the inherent complexity and variety of access control

mechanisms in DeFi applications make it difficult to develop a universally applicable rule for all forms of faulty access control.

**6.3.5 Refinement A2 - Addressing False Positives Stemming from Fixed Recipients.** Refinement A2 focuses on false positives arising due to fixed recipients in contract transactions. A number of contracts enable permissionless transfers to predetermined destinations. For example, a widely-used function called `harvest`<sup>3</sup> allows any user to collect compound interest to a designated contract. To tackle this issue, we implement a rule in the traversal process to examine all data sources associated with the asset flow destination, confirming whether they can be controlled by transaction call data.

**6.3.6 Refinement A3 - Eliminating False Positives Linked to Asset Swaps.** Refinement A3 is designed to eliminate false positives that occur in asset swap transactions. In a token swap scenario, the returning asset flow might seemingly lack access control. To address this, we attempt to group asset flows based on their associated data sources related to the transfer amount, ensuring a minimum of one controlled flow in each group.

**6.3.7 Challenges.** Some applications leverage signature validation as the access control method, in which users can prove to the contract that they have access to the vault by providing signatures from the owner. Such implicit access control is hard to capture in the traversal. Furthermore, while profiting is almost always the ultimate goal of a DeFi attack, as demonstrated by the DaoMaker attack, faulty access control can also occur on functions without asset flows, making it even more challenging to design a general rule for detection. These challenges and insights highlight the complexity of DeFi applications and the need for developing more sophisticated techniques in future works to better identify and mitigate the risks associated with faulty access control.

## 6.4 Price Manipulation

Table 3 presents the evaluation results of price manipulation attacks. In the assessment of the *Attack* dataset, CLUE identified 53 malicious transactions in total, with 1 attack transaction undetected, resulting in a FNR of 1.85%. The undetected transaction is part of a multi-transaction attack event, which is out of the scope of this study. In the *High-Gas* dataset, the generic traversal rule flagged 753 transactions, yielding a high false positive rate of 70.05%. In the *Regular* dataset, it flagged 1,579 transactions, resulting in a false positive rate of 7.90%.

Upon examination of these false positives, we discover that the generic rule does not perform well in (i) transactions that consume significant amounts of gas, particularly those involving flash swap actions between multiple swap pools; and (ii) specific DeFi actions, such as claiming and compounding rewards. To mitigate this issue, we introduce the following heuristics.

**6.4.1 Refinement P1 - Detecting Irregular Price Fluctuation.** We flag swap pool contracts within the transaction call traces and analyze the relative price fluctuations of these pools to detect any irregular price shifts. We accomplish this by determining the proportion of the alteration in the token balance within the swap pool relative to the aggregate token balance. It is crucial to note that most price

<sup>3</sup><https://docs.beefy.finance/developer-documentation/strategy-contract#harvest>

**Table 3: Price manipulation evaluation. The refined rule yields a high true positive rate (94.44%) and a relatively low false negative rate (5.56%) in the *Attack* dataset, with false negatives resulting from low profit margin and multi-transaction cases. In non-attack datasets, the true negative rates are significantly improved (98.51%) for *High-Gas* and (99.48%) for *Regular* after incorporating P1 and P2. The remaining false positives are primarily caused by arbitrage, complex transactions, and add/remove liquidity actions.**

Dataset	Attack	Non-attack	
		High-Gas	Regular
Size	54	1,075	19,989
Gas Cost	6.89 ± 3.37M	2.14 ± 1.38M	0.24 ± 0.26M
Generic Rule (cf. Section 5.5)			
Traversal Time	32 ± 17ms	7 ± 27ms	2.2 ± 1.1ms
TP (%)	53 (98.15%)	-	-
FN (%)	1 (1.85%)	-	-
Multi-tx	1/1	-	-
TN (%)	-	322 (29.95%)	18,410 (92.10%)
FP (%)	-	753 (70.05%)	1,579 (7.90%)
Refined Rule (Generic Rule + Refinement P1, P2)			
Traversal Time	47 ± 23ms	10 ± 24ms	2.4 ± 1.5ms
TP (%)	51 (94.44%)	-	-
FN (%)	3 (5.56%)	-	-
Low profit	2/3	-	-
Multi-tx	1/3	-	-
TN (%)	-	1,059 (98.51%)	19,886 (99.48%)
FP (%)	-	16 (1.49%)	103 (0.52%)
Arbitrage	-	0/16	29/103
Complex DeFi	-	10/16	2/103
Add/Remove liquidity	-	6/16	72/103

manipulation attacks follow a *swap-and-borrow* pattern, where significant influence on the relative price through swaps is essential for the exploitation process. High-slippage swaps are uncommon for typical users. By focusing on swap pool contracts, we avoid false positive examples caused by depositing or withdrawing tokens. For example, a function called `doHardWork` interacts with Harvest Finance contracts,<sup>4</sup> performing complicated actions that trigger the price manipulation rule while the swap amount remains small. This refinement effectively excludes such transactions.

**6.4.2 Refinement P2 - Assessing Absolute Value Changes.** In Refinement P2, we calculate the absolute USD value changes of swap pools by utilizing the asset flows in EPG and historical token prices from an online database. This approach is especially effective in eliminating false positive cases in small-scale arbitrage transactions and intricate DeFi transactions, as the compounding process only trades existing profits. By monitoring and evaluating the absolute value changes, we can effectively differentiate between legitimate transactions and potential price manipulation attempts. This refinement enhances the overall accuracy of the detection process.

<sup>4</sup>An example transaction of the `doHardWork` function: `0xcb4e7c976b4751cd93e758001135612bdd3da276b2f81814c924391d7e985f55`

**6.4.3 Refined Performance.** After applying the domain-specific improvements, CLUE demonstrates a FNR of 5.56% and FPR of 1.49% and 0.52% in the *High-Gas* and *Regular* datasets, respectively. The false positive cases in the *High-Gas* dataset primarily fall into two categories: *add/remove liquidity* and *arbitrage*, accounting for approximately 70% and 30% of the false positive cases, respectively. In the *Regular* dataset, 10 false positive cases resulted from large-scale swap operations in complex DeFi transactions, while 6 transactions were categorized as *add/remove liquidity*.

**6.4.4 False Negative Analysis of the Refined Rule.** In the *Attack* dataset, two transactions are marked by low profit margins, leading to their false negative classification.

**6.4.5 False Positive Analysis of the Refined Rule.** After applying the refined rule in the *High-Gas* dataset, 10 of the false positive cases resulted from large-scale swap operations in complex DeFi transactions, including *deposit*, *withdraw* and *compounding* while other 6 transactions are categorized as *add/remove liquidity*. After applying the refined rule in the *Regular* dataset, the false positive cases fell into two categories: *add/remove liquidity* and *arbitrage*, accounting for approximately 70% and 28% among the false positive cases, respectively. The former type contains actions of adding liquidity to or removing liquidity from swap pools, which performs swap operations at the beginning. The former type encompasses large-scale *arbitrage* transactions with significant earnings. These transactions profit from the price difference between swap pools.

**6.4.6 Challenges.** Detecting price manipulation attacks in DeFi applications is a challenging task due to the complexity and diversity of the underlying transactions. By incorporating domain-specific knowledge, CLUE not only improved its accuracy but also demonstrated its adaptability and extensibility. However, some challenges remain, such as detecting multi-transaction attack events and distinguishing between large-scale legitimate swap operations and price manipulation attempts. Further research and refinement are necessary to develop more sophisticated techniques to tackle these challenges effectively.

**6.4.7 Summary.** CLUE exhibits remarkable performance in detecting price manipulation attacks using the refined rule, with a FNR of 5.56% and FPR of 1.49% and 0.52% in the *High-Gas* and *Regular* datasets, respectively. Furthermore, the incorporation of domain-specific knowledge and the refined filtering mechanisms have demonstrated the system’s adaptability and extensibility in addressing the complex landscape of DeFi applications.

## 6.5 Traversal Performance Overhead

Our time performance evaluation focuses on the overhead associated with graph traversals. As demonstrated in Tables 1, 2, and 3, for attack transactions, CLUE completes detection within an average time of 1s. In the *Regular* dataset, traversal time averages below 100ms, with a majority (89.6%) taking less than 20ms. It is crucial to mention that our prototype has not been optimized for performance. Consequently, the refined rule for faulty access control detection applied to the *High-Gas* dataset, which represents transactions with complex logic, requires an average of 8s. The remaining traversals on the *High-Gas* dataset finishes under 1s

on average. For reference, the block interval of Ethereum is 12s. Our evaluation highlights the efficacy of our traversal approach, demonstrating its strong potential for online detection scenarios.

## 7 RELATED WORK

**Graph-based Static Program Analysis.** Graphs have become the fundamental building blocks in the field of program analysis. In tasks such as program optimization and vulnerability discovery, the utilization of various types of graphs, including AST, CFG, and PDG, is essential for achieving accurate and reliable results. Combining AST, CFG, and PDG, Yamaguchi *et al.* [31] first introduce the concept of code property graph (CPG), which represents program source code as a property graph. Such a comprehensive view of code enables rigorous identification of vulnerabilities through graph traversals. CPG has been shown to be effective in identifying buffer overflows, integer overflows, format string vulnerabilities, and memory disclosures [31]. Giesen *et al.* [11] apply the CPG approach to smart contracts and propose HCC. HCC models control-flows and data-flows of a given smart contract statically as a CPG, which allows efficient detection and mitigation of integer overflow and reentrancy vulnerabilities. Inspired by the previous studies, we propose the EPG to model the dynamic contract execution details as a property graph. Compared to the static approaches, the EPG captures runtime information exposed from the concrete executions and hence complements the contract security analysis, particularly in the online and postmortem scenarios.

**Smart Contract Dynamic Analysis.** Previous studies in the field of smart contract dynamic analysis have primarily focused on two key directions, (i) online attack detection and (ii) forensic analysis.

- **Online Attack Detection.** Grossman *et al.* [12] develop a polynomial online algorithm for checking if an execution is effectively callback free, a property for detecting reentrancy vulnerabilities. Rodler *et al.* [25] introduce Sereum, a runtime solution to detect smart contract reentrancy vulnerabilities. Sereum exploits dynamic taint tracking to monitor data-flows during contract execution and applies to various types of reentrancy vulnerabilities. Chen *et al.* [7] develop SODA, an online framework for detecting various smart contract attacks.
- **Forensic analysis.** Perez and Livshits [21] propose a Datalog-based formulation for performing analysis over EVM execution traces and conduct a large-scale evaluation on 23,327 vulnerable contracts. Zhou *et al.* [34] undertake a measurement study on 420M Ethereum transactions, constructing transaction trace into action and result trees. The action tree gives information of contract invocations, while the result tree provides asset transfer data, which are then compared against predefined attack patterns. Zhang *et al.* [32] design TxSPECTOR, a logic-driven framework to investigate Ethereum transactions for attack detection. TxSPECTOR encodes the transaction trace into logic relations and identifies attacks following user-specified detection rules.

**Smart Contract and DeFi Attacks.** There has been a growing body of literature examining the prevalence of smart contract attacks, with a particular emphasis on those targeting DeFi platforms. Qin *et al.* [23] study the first two flash loan attacks and propose a numerical optimization framework that allows optimizing DeFi attack parameters. Li *et al.* [16] conduct a comprehensive analysis

of the real-world DeFi vulnerabilities. Zhou *et al.* [33] present a reference framework that categorizes 181 DeFi attacks occurring between April 2018 and April 2022, related academic papers, as well as security audit reports into a taxonomy.

## 8 CONCLUSION

In this paper, we have presented a versatile dynamic analysis framework specifically tailored for the EVM, shedding light on the pressing need to improve smart contract security in today’s rapidly expanding DeFi landscape. Our proposed approach, centered around the new EPG and graph traversal technique, offers a novel, efficient, and effective method for identifying potential smart contract attacks, transcending limitations of other techniques by capturing valuable runtime information. The successful detection of a zero-day vulnerability affecting Uniswap, along with solid true positive rates, highlight the strength of our framework.

## REFERENCES

- [1] Alfred V Aho, Monica S Lam, Ravi Sethi, and Jeffrey D Ullman. 2007. *Compilers: principles, techniques, & tools*. Pearson Education India.
- [2] Frances E Allen. 1970. Control flow analysis. *ACM Sigplan Notices* 5, 7 (1970), 1–19.
- [3] David Binkley. 2007. Source code analysis: A road map. *Future of Software Engineering (FOSE’07) (2007)*, 104–119.
- [4] Priyanka Bose, Dipanjan Das, Yanju Chen, Yu Feng, Christopher Kruegel, and Giovanni Vigna. 2022. Sailfish: Vetting smart contract state-inconsistency bugs in seconds. In *2022 IEEE Symposium on Security and Privacy (SP)*. IEEE, 161–178.
- [5] Michael Burke and Ron Cytron. 1986. Interprocedural dependence analysis and parallelization. *ACM Sigplan Notices* 21, 7 (1986), 162–175.
- [6] Ethan Cecchetti, Siqui Yao, Haobin Ni, and Andrew C Myers. 2021. Compositional security for reentrant applications. In *2021 IEEE Symposium on Security and Privacy (SP)*. IEEE, 1249–1267.
- [7] Ting Chen, Rong Cao, Ting Li, Xiapu Luo, Guofei Gu, Yufei Zhang, Zhou Liao, Hang Zhu, Gang Chen, Zheyuan He, et al. 2020. SODA: A Generic Online Detection Framework for Smart Contracts. In *NDSS*.
- [8] Josselin Feist, Gustavo Grieco, and Alex Groce. 2019. Slither: a static analysis framework for smart contracts. In *2019 IEEE/ACM 2nd International Workshop on Emerging Trends in Software Engineering for Blockchain (WETSEB)*. IEEE, 8–15.
- [9] Jeanne Ferrante, Karl J Ottenstein, and Joe D Warren. 1987. The program dependence graph and its use in optimization. *ACM Transactions on Programming Languages and Systems (TOPLAS)* 9, 3 (1987), 319–349.
- [10] Asem Ghaleb and Karthik Pattabiraman. 2020. How effective are smart contract analysis tools? evaluating smart contract static analysis tools using bug injection. In *Proceedings of the 29th ACM SIGSOFT International Symposium on Software Testing and Analysis*. 415–427.
- [11] Jens-Rene Giesen, Sebastien Andreina, Michael Rodler, Ghassan O Karame, and Lucas Davi. 2022. Practical Mitigation of Smart Contract Bugs. *arXiv preprint arXiv:2203.00364* (2022).
- [12] Shelly Grossman, Ittai Abraham, Guy Golan-Gueta, Yan Michalevsky, Noam Rinetzky, Mooly Sagiv, and Yoni Zohar. 2017. Online detection of effectively callback free objects with applications to smart contracts. *Proceedings of the ACM on Programming Languages* 2, POPL (2017), 1–28.
- [13] Eyal Hertzog, Guy Benartzi, and Galia Benartzi. 2017. Bancor protocol. *Continuous Liquidity for Cryptographic Tokens through their Smart Contracts*. Available online: [https://storage.googleapis.com/website-bancor/2018/04/01ba8253-bancor\\_protocol\\_whitepaper\\_en.pdf](https://storage.googleapis.com/website-bancor/2018/04/01ba8253-bancor_protocol_whitepaper_en.pdf) (accessed on 6 June 2020) (2017).
- [14] Susan Horwitz, Jan Prins, and Thomas Reps. 1988. On the adequacy of program dependence graphs for representing programs. In *Proceedings of the 15th ACM SIGPLAN-SIGACT symposium on Principles of programming languages*. 146–157.
- [15] Susan Horwitz and Thomas Reps. 1992. The use of program dependence graphs in software engineering. In *Proceedings of the 14th international conference on Software engineering*. 392–411.
- [16] Wenkai Li, Jiuyang Bu, Xiaoqi Li, Hongli Peng, Yuanzheng Niu, and Xianyi Chen. 2022. A Survey of DeFi Security: Challenges and Opportunities. *arXiv preprint arXiv:2206.11821* (2022).
- [17] Loi Luu, Duc-Hiep Chu, Hrishi Olickel, Prateek Saxena, and Aquinas Hobor. 2016. Making smart contracts smarter. In *Proceedings of the 2016 ACM SIGSAC conference on computer and communications security*. 254–269.
- [18] Mark Mossberg, Felipe Manzano, Eric Hennenfent, Alex Groce, Gustavo Grieco, Josselin Feist, Trent Brunson, and Artem Dinaburg. 2019. Manticore: A user-friendly symbolic execution framework for binaries and smart contracts. In *2019 34th IEEE/ACM International Conference on Automated Software Engineering (ASE)*. IEEE, 1186–1189.
- [19] Bernhard Mueller. 2018. Smashing ethereum smart contracts for fun and real profit. *HITB SECCONF Amsterdam 9* (2018), 54.
- [20] Satoshi Nakamoto. 2008. Bitcoin: A peer-to-peer electronic cash system. <https://bitcoin.org/bitcoin.pdf>.
- [21] Daniel Perez and Benjamin Livshits. 2021. Smart Contract Vulnerabilities: Vulnerable Does Not Imply Exploited. In *USENIX Security Symposium*. 1325–1341.
- [22] Kaihua Qin, Liyi Zhou, Pablo Gamito, Philipp Jovanovic, and Arthur Gervais. 2021. An empirical study of defi liquidations: Incentives, risks, and instabilities. In *Proceedings of the 21st ACM Internet Measurement Conference*. 336–350.
- [23] Kaihua Qin, Liyi Zhou, Benjamin Livshits, and Arthur Gervais. 2021. Attacking the defi ecosystem with flash loans for fun and profit. In *International Conference on Financial Cryptography and Data Security*. Springer, 3–32.
- [24] Meng Ren, Fuchen Ma, Zijing Yin, Ying Fu, Huizhong Li, Wanli Chang, and Yu Jiang. 2021. Making smart contract development more secure and easier. In *Proceedings of the 29th ACM Joint Meeting on European Software Engineering Conference and Symposium on the Foundations of Software Engineering*. 1360–1370.
- [25] Michael Rodler, Wenting Li, Ghassan Karame, and Lucas Davi. 2019. Sereum: Protecting Existing Smart Contracts Against Re-Entrancy Attacks. In *NDSS*.
- [26] Marko A Rodriguez. 2015. The gremlin graph traversal machine and language (invited talk). In *Proceedings of the 15th Symposium on Database Programming Languages*. 1–10.
- [27] Marko A Rodriguez and Peter Neubauer. 2012. The graph traversal pattern. In *Graph data management: Techniques and applications*. IGI global, 29–46.
- [28] Muyao Shen. 2021. Crypto fundraising dao loses over \$7M in latest crypto exploit. <https://www.coindesk.com/markets/2021/08/12/crypto-fundraising-dao-loses-over-7m-in-latest-crypto-exploit/>
- [29] Sergei Tikhomirov, Ekaterina Voskresenskaya, Ivan Ivanitskiy, Ramil Takhaviev, Evgeny Marchenko, and Yaroslav Alexandrov. 2018. Smartcheck: Static analysis of ethereum smart contracts. In *Proceedings of the 1st International Workshop on Emerging Trends in Software Engineering for Blockchain*. 9–16.
- [30] Petar Tsankov, Andrei Dan, Dana Drachler-Cohen, Arthur Gervais, Florian Buenzli, and Martin Vechev. 2018. Securify: Practical security analysis of smart contracts. In *Proceedings of the 2018 ACM SIGSAC Conference on Computer and Communications Security*. 67–82.
- [31] Fabian Yamaguchi, Nico Golde, Daniel Arp, and Konrad Rieck. 2014. Modeling and discovering vulnerabilities with code property graphs. In *2014 IEEE Symposium on Security and Privacy*. IEEE, 590–604.
- [32] Mengya Zhang, Xiaokuan Zhang, Yinqian Zhang, and Zhiqiang Lin. 2020. {TXSPECTOR}: Uncovering attacks in ethereum from transactions. In *29th USENIX Security Symposium (USENIX Security 20)*. 2775–2792.
- [33] Liyi Zhou, Xihan Xiong, Jens Ernstberger, Stefanos Chaliasos, Zhipeng Wang, Ye Wang, Kaihua Qin, Roger Wattenhofer, Dawn Song, and Arthur Gervais. 2022. SoK: Decentralized Finance (DeFi) Attacks. *Cryptology ePrint Archive* (2022).
- [34] Shunfan Zhou, Malte Möser, Zheming Yang, Ben Adida, Thorsten Holz, Jie Xiang, Steven Goldfeder, Yinzi Cao, Martin Plattner, Xiaojun Qin, et al. 2020. An ever-evolving game: Evaluation of real-world attacks and defenses in ethereum ecosystem. In *29th USENIX Security Symposium (USENIX Security 20)*. 2793–2810.

## A MONOX PROTOCOL HACK CASE STUDY

On the 30th of November, 2021, a DeFi protocol MonoX was targeted by one Ethereum transaction causing a total loss of 31M USD to liquidity providers.<sup>5</sup> MonoX is an Automated Market Maker protocol that holds more than two tokens in the same liquidity pool. Therefore, MonoX relies on a price oracle for market price discovery. This internal oracle allows updating its price within a single transaction. Related work has shown that such oracles can be manipulated through e.g., sizable transaction volumes, readily available through flash loans [23].

While this oracle manipulation may appear trivial, there are two main difficulties in executing the MonoX attack. First, from the transaction trace it is non-obvious that the attack carried out an oracle manipulation. Second, the oracle manipulation requires the concatenation of a second issue to drain the entire MonoX smart contract. We will dissect the details in the following and start

<sup>5</sup>Transaction hash: 0x9f14d093a2349de08f02fc0fb018dadb449351d0cdb7d0738ff69cc6fe f5f299

```

1  contract Monoswap {
2      function removeLiquidity (address _token, uint256 liquidity,
3          address to, uint256 minVcashOut, uint256 minTokenOut
4      ) external returns(uint256 vcashOut, uint256 tokenOut) {
5          (vcashOut, tokenOut) = _removeLiquidityHelper (_token, liquidity, to, minVcashOut,
6              minTokenOut, false);
7      }
8
9      function swapExactTokenForToken(
10         address tokenIn,
11         address tokenOut,
12         uint amountIn,
13         uint amountOutMin,
14         address to,
15         uint deadline
16     ) external virtual ensure(deadline) returns (uint amountOut) {
17         amountOut = swapIn(tokenIn, tokenOut, msg.sender, to, amountIn);
18         require(amountOut >= amountOutMin, 'MonoX:INSUFF_OUTPUT');
19     }
20 }

```

Listing 2: MonoX vulnerable contract

```

1  {
2      "gas": 4684892,
3      "failed": false,
4      "returnValue": "",
5      "structLogs": [
6          ...,
7          {
8              "pc": 1164,
9              "op": "SSTORE",
10             "gas": 5718423,
11             "gasCost": 20000,
12             "depth": 2,
13             "stack": [
14                 "0xd0e30db0",
15                 "0x3d2",
16                 "0x16345785d8a0000",
17                 "0x16345785d8a0000",
18                 "0xbb1cc82d95791a1a9ca876fa9a5c6956b2ce21989bd57cca42dcdd3cbf705c6"
19             ],
20             "memory": [
21                 "00000000000000000000000000000000f079d7911c13369e7fd85607970036d2883afcfd",
22                 "0000000000000000000000000000000000000000000000000000000000000003",
23                 "00000000000000000000000000000000000000000000000000000000000000060"
24             ],
25             "storage": {
26                 "0bb1cc82d95791a1a9ca876fa9a5c6956b2ce21989bd57cca42dcdd3cbf705c6":
27                 ↪ "0000000000000000000000000000000000000000000000000000000000000016345785d8a0000"
28             }
29         },
30         ...,
31     ]
32 }

```

Listing 3: Transaction trace of the MonoX attack transaction. "structLogs" is an array recording the EVM stack, memory, and storage, following the execution of every opcode. The presented transaction trace captures in total 596,302 opcodes.

by showing the related vulnerable contract code in Listing 2. The high-level flow of the MonoX attack operates as follows.

- ① The attacker  $\mathcal{A}$  exchanges 0.1 WETH for 79.9 MONO on Monoswap. This is a regular exchange following the market price prior to the attack.
- ②  $\mathcal{A}$  drains all MONO tokens from Monoswap, while not affecting other tokens in the exchange. The `removeLiquidity` function (cf. Listing 2) does not have a permission check. Therefore,  $\mathcal{A}$  is able to remove liquidity for any liquidity
- ③  $\mathcal{A}$  adds a tiny amount ( $2 \times 10^{-10}$ ) of MONO liquidity into Monoswap. Such shallow liquidity allows  $\mathcal{A}$  to effectively manipulate the MONO price in step ④.
- ④  $\mathcal{A}$  repeats exchanging MONO for MONO at Monoswap. The `swapExactTokenForToken` function allows exchanges between the same token. Because the price oracle updates atomically after every swap in Monoswap, the MONO price is increased by  $161,700,000,000\times$  after 55 swaps of MONO.

```

1  pragma solidity ^0.8.0;
2
3  contract DataFlow {
4      uint totalBalance;
5      mapping(address => uint) balances;
6      address callee;
7
8      fallback() external payable {
9          totalBalance = address(this).balance;
10         balances[msg.sender] += msg.value;
11         callee.call(abi.encode(totalBalance));
12     }
13 }

```

Listing 4: Example for CLUE data-flow tracking.

- ⑤ The price manipulation in step ④ increases the price of MONO.  $\mathcal{A}$  purchased MONO in step ①, which now has a value that is 161,700,000,000× higher than before the attack. The attacker can hence capitalize on the attack by selling MONO against the other tokens in the MonoX exchange.

## B IMPLEMENTATION DETAILS

### B.1 Overview

CLUE supports both online and offline modes.

**Online Mode** In the online mode, CLUE is integrated with a full node, which receives unconfirmed transactions from the P2P network. CLUE injects a callback function into EVM. This injected callback function, also known as EVM tracing, is supported by most EVM implementations (e.g., [go-ethereum](#)). Our design hence ensures minimal code change on the EVM side. While executing a transaction, EVM invokes the callback function and exposes the runtime information (e.g., the opcode at every step) for further investigation.

**Offline Mode** In the offline mode, CLUE takes the execution trace of a transaction, provided by an archive node, as the input to recover the runtime details. To be compatible with the callback injection design, we devise a trace simulator, which allows the EVM emulator to inject the same callback function as the online mode. The trace simulator parses the transaction execution trace and invokes the callback function as if the transaction is executed in the real EVM.

By tracking the transaction execution, CLUE builds the data, control, and asset flows, from which CLUE further generates the CTG, DCFG, DDG and constructs the EPG.

### B.2 Data-Flow Tracking

To track data flows, the EVM emulator employed in CLUE maintains its own stack, memory, and storage, where data tags are stored. These data tags indicate the sources of corresponding data in EVM. For instance, the emulator pushes a data tag marked as storage to the emulated stack when the EVM loads a storage variable to its stack. We include the detailed location information in data tags (e.g., contract address and slot for storage) if applicable. Data tags propagate following copy, logical, and arithmetical instructions. A data tag can be multisource, when it is, for example, the outcome of an arithmetical operation on variables from different sources. Specially, for contract storage, we also track the data-flow for the storage slot. CLUE

moreover captures the implicit data flow that is not directly observable. In the DataFlow contract, the fallback function accepts ETH and updates the storage variable totalBalance (line 9, Listing 4). It appears that the data flow is from address(this).balance to totalBalance. However, the contract balance is incremented by msg.value when fallback is invoked. Therefore, there exists a latent data flow from msg.value to totalBalance. CLUE tracks account balances and call values as special variables and hence can capture such implicit data flow. As discussed in Section 4.2.3, CLUE maintains the full change history of contract storage and account balance. By following the input and output of contract invocations, CLUE also tracks cross-contract data flows. For example, in Listing 4, totalBalance is used as a parameter of the call to callee (line 11).

### B.3 Control-Flow Tracking

EVM implements program control through code jumps (cf. Section 4.2.2). CLUE meticulously tracks the control flows by recording the code jump opcodes, specifically JUMP and JUMPI, as well as the corresponding basic blocks. In the case of conditional jumps (JUMPI), CLUE also records the data flows of the jump conditions. This information is crucial for the identification of vulnerabilities, including reentrancy, as discussed in Section 5.3.

### B.4 Asset-Flow Tracking

Tracking ETH transfers is a relatively straightforward process within CLUE. CLUE filters the relevant opcodes (i.e., CALL, CREATE, CREATE2, and SELFDESTRUCT) and then determines if there is an ETH transfer.

In contrast, tracking the transfers of contract-realized assets is more complex due to the diverse range of contract implementations. In this work, we mainly focus on ERC-20, the de facto standard of fungible tokens on the EVM-compatible blockchains, especially in the DeFi ecosystem. The ERC-20 standard defines a Transfer event, which is emitted upon the execution of a token transfer. By matching the Transfer event during transaction execution, we record the ERC-20 transfer when a match is found. This method can also be applied to non-fungible token standards, such as ERC-721.

It should be noted that the event matching mechanism may introduce false positives. For example, an adversary might create a malicious contract that emits the Transfer event without actually transferring assets, in an attempt to confuse the transaction analysis. To mitigate this, additional filtering conditions can be employed, such as an allowlist that only tracks contracts of interest.